# Adai: Separating the Effects of Adaptive Learning Rate and Momentum Inertia

Zeke Xie<sup>1,2</sup>, Xinrui Wang<sup>3,1</sup>, Huishuai Zhang<sup>4</sup>, Issei Sato <sup>1,2</sup> and Masashi Sugiyama<sup>2,1</sup>

<sup>1</sup>The University of Tokyo
<sup>2</sup>RIKEN Center for AIP
<sup>3</sup>ByteDance AI Lab
<sup>4</sup>Microsoft Research Asia
xie@ms.k.u-tokyo.ac.jp
wangxinrui.233@bytedance.com
Huishuai.Zhang@microsoft.com
{sato,sugi}@k.u-tokyo.ac.jp

#### Abstract

Adaptive Momentum Estimation (Adam), which combines Adaptive Learning Rate and Momentum, is the most popular stochastic optimizer for accelerating training of deep neural networks. But Adam often generalizes significantly worse than Stochastic Gradient Descent (SGD). It is still mathematically unclear how Adaptive Learning Rate and Momentum affect saddle-point escaping and minima selection. Based on the diffusion theoretical framework, we separate the effects of Adaptive Learning Rate and Momentum on saddle-point escaping and minima selection. We find that SGD escapes saddle points very slowly along the directions of small-magnitude eigenvalues of the Hessian. We prove that Adaptive Learning Rate can make learning dynamics near saddle points approximately Hessian-independent, but cannot select flat minima as SGD does. In contrast, Momentum provides a momentum drift effect to help passing through saddle points, and almost does not affect flat minima selection. This mathematically explains why SGD (with Momentum) generalizes better, while Adam generalizes worse but converges faster. Motivated by the diffusion theoretical analysis, we design a novel adaptive optimizer named Adaptive Inertia Estimation (Adai), which uses parameterwise adaptive inertia to accelerate training and provably favors flat minima as much as SGD. Our real-world experiments demonstrate that Adai can converge similarly fast to Adam, but generalize significantly better. Adai even generalizes better than SGD.

#### 1 Introduction

Adaptive gradient methods, such as AdaGrad (Duchi et al., 2011), RMSprop (Hinton et al., 2012), Adadelta (Zeiler, 2012) and Adam (Kingma and Ba, 2015), are a class of dominated methods to accelerate training of deep neural networks. Among them, Adam, which combines Adaptive Learning Rate and Momentum together, is the most popular one. However, Adam often has significantly worse generalizability than SGD (with Momentum) (Wilson et al., 2017).

Recent years, a few variants of Adam are proposed to fix hidden problems in Adam. Loshchilov and Hutter (2017) proposed AdamW as the correct implementation of Adam with Decoupled Weight Decay. Reddi et al. (2019) argued that the updating rules of Adam may lead to sub-optimal points, and proposed AMSGrad. With increasing understanding of Adam, some researchers started to believe controlling the adaptiveness of learning rates may improve

generalization. A few Adam variants have been discussed along this line, such as Yogi (Zaheer et al., 2018), Adabound (Luo et al., 2019), Padam (Chen and Gu, 2018). Some of the variants (Luo et al., 2019; Chen and Gu, 2018) introduced extra hyperparameters into the algorithms, which require more fine-tuning effort. Moreover, none of these Adam variants can consistently generalize as well as SGD in wide practice.

The diffusion theory is an important approach to understanding the dynamics of stochastic optimizers. A few works (Sato and Nakagawa, 2014; Raginsky et al., 2017; Zhang et al., 2017; Xu et al., 2018) discussed a relatively simplified case, the diffusion process of Stochastic Gradient Langevin Dynamics (SGLD). A few papers (Jastrzębski et al., 2017; Achille and Soatto, 2019) studied how minima selection depends on the learning rate, the batch size and the minima flatness, under the isotropic noise approximation. Zhu et al. (2019) revealed that the anisotropic diffusion of SGD leads to flat minima qualitatively better than the isotropic one of SGLD. Hu et al. (2019) quantitatively showed that the mean escape time of SGD exponentially depends on the inverse learning rate. Xie et al. (2020) formulated a refined quantitative theory for the minima selection mechanism of SGD, which exponentially depends on the eigenvalues of the Hessian at minima and the ratio of the batch size and learning rate. However, none of these works has quantitatively analyzed the continuous-time diffusion process of SGD near saddle points. Li et al. (2017) analyzed Stochastic Differential Equation of adaptive gradient methods, including Adam. But it did not elucidate the diffusion process of Adam in matters of escaping either sharp minima or saddle points.

In this paper, we theoretically reveal that Adam is better at saddle-point escaping but worse at flat minima selection. In our diffusion analysis, the minima sharpness is reflected by the eigenvalue of the Hessian at minima along the escape direction. Is it possible to accelerate saddle-point escaping without damaging learning flat minima? Yes. We design a novel adaptive mechanism, which is essentially different from adaptive gradient methods. We do not element-wisely adjust learning rates, but element-wisely adjust the momentum hyperparameter (inertia) instead. We mainly have three contributions in this paper:

- We elucidate the diffusion process of SGD near saddle points.
- We theoretically separate the effects of Adaptive Learning Rate and Momentum Inertia. Adam can escape saddle points efficiently, because Adam dynamics near saddle points is approximately Hessian-independent. Adam does not favor flat minima as much as SGD, because Adam is less sensitive to the Hessian at minima than SGD.
- Adai: We propose the element-wisely adaptive inertia method. Adai can provide an approximately Hessian-independent momentum drift to accelerate training, and provably favors flat minima as much as SGD.

In Section 2, we theoretically analyze SGD diffusion near saddle points. In Section 3, we theoretically analyze Momentum and Adam diffusion, and separate the effects of Adaptive Learning Rate and Momentum on saddle-point escaping and minima selection. In Section 4, we propose Adai. In Section 5, we conduct experiments to compare Adai with Adam and SGD with Momentum. We display the test performance in Table 1. In Section 6, we conclude our main work.

#### 1.1 Prerequisites for SGD Diffusion Theory

We briefly review the diffusion theoretical framework of Xie et al. (2020) that quantitatively demonstrates how SGD searches flat minima based on the diffusion theoretical framework. We denote the data samples as  $S = \{(x_j, y_j)\}_{j=1}^N$ , the model parameters as  $\theta$ , the learning rate as  $\eta$ , the batch size as B, and the loss function over one sample  $z_j = (x_j, y_j)$  as  $L(\theta, z_j)$ . For simplicity, we denote the training loss of the training dataset as  $L(\theta)$ . SGD dynamics

<sup>&</sup>lt;sup>1</sup>When we talk about saddle points, we mean strict saddle points in this paper.

Table 1: Test performance comparison. We report the mean and the standard deviations of the optimal test errors and the standard deviation computed over three runs on CIFAR-10 and CIFAR-100, and the optimal test errors over one run on ImageNet. We use \* to denote the hyperparameter settings which make Adai converge similarly fast to Adam.

DATASET	Model	Adai	SGD M	Adai *	Adam	AMSGRAD	AdamW
CIFAR-10	ResNet18	4.800.15	$4.98_{0.01}$	$5.53_{0.11}$	$6.46_{0.11}$	$6.75_{0.20}$	6.59 <sub>0.13</sub>
	VGG16	$6.24_{0.23}$	$6.42_{0.02}$	$6.80_{0.14}$	$7.85_{0.18}$	$8.05_{0.13}$	$7.55_{0.20}$
CIFAR-100	DenseNet121	$19.52_{0.20}$	$19.62_{0.13}$	$21.87_{0.03}$	$25.36_{0.09}$	$25.52_{0.29}$	$25.05_{0.26}$
	GoogLeNet	$20.60_{0.32}$	$21.05_{0.14}$	$22.84_{0.21}$	$26.63_{0.44}$	$27.49_{0.27}$	$26.24_{0.66}$
IMAGENET (TOP1)	ResNet50	23.20	23.51	27.09	27.13	28.08	27.47
$ImageNet({\tiny \texttt{Top5}})$	ResNet50	6.62	6.82	8.89	9.18	9.48	9.29

can be written as

$$\theta_{t+1} = \theta_t - \eta \frac{\partial L(\theta)}{\partial \theta} + \eta C(\theta)^{\frac{1}{2}} \zeta_t, \tag{1}$$

where  $\zeta_t \sim \mathcal{N}(0, I)$ , I is the identity matrix, and  $C(\theta)$  represents the gradient noise covariance matrix. The stochastic gradient noise is defined by  $\frac{\partial \hat{L}(\theta)}{\partial \theta} - \frac{\partial L(\theta)}{\partial \theta}$ , where  $\hat{L}(\theta)$  is the loss of a minibatch. According to Central Limit Theorem (Gnedenko et al., 1954), the mean of many finite-variance random variables converges to a Gaussian distribution. As the stochastic gradient noise is finite in practice, we consider stochastic gradient noise is anisotropic Gaussian,  $\mathcal{N}(0, C(\theta))$ . Simsekli et al. (2019) reports that stochastic gradient noise is more like heavy-tailed Lévy noise. However, the empirical evidence of Simsekli et al. (2019) supports Lévy noise only if stochastic gradient noise obeys the same distribution across parameters. This hidden isotropic assumption is unreasonable in Langevin Dynamics. We empirically verify that the stochastic gradient noise is Gaussian, while stochastic gradient is heavy-tailed, seen in Appendix C.

Let us replace  $\eta$  by dt as unit time. The continuous-time dynamics of SGD is written as

$$d\theta = -\frac{\partial L(\theta)}{\partial \theta} dt + [2D(\theta)]^{\frac{1}{2}} dW_t, \tag{2}$$

where  $dW_t \sim \mathcal{N}(0, Idt)$  and  $D(\theta) = \frac{\eta}{2}C(\theta)$ . The Fokker-Planck equation of deep learning dynamics is written as

$$\frac{\partial P(\theta, t)}{\partial t} = \nabla \cdot [P(\theta, t) \nabla L(\theta)] + \nabla \cdot \nabla D(\theta) P(\theta, t)$$
(3)

$$= \sum_{i} \frac{\partial}{\partial \theta_{i}} \left[ P(\theta, t) \frac{\partial L(\theta)}{\partial \theta_{i}} \right] + \sum_{i} \sum_{j} \frac{\partial^{2}}{\partial \theta_{i} \partial \theta_{j}} D_{ij}(\theta) P(\theta, t), \tag{4}$$

where  $\nabla$  is the gradient operator,  $\nabla$ · is the divergence operator, and  $D_{ij}$  is the element in the *i*-th row and *j*-th column of D. Different learning dynamics indicates different diffusion matrix. We note that the dynamical time t in the continuous-time dynamics is equal to the product of the number of iterations T and the learning rate  $\eta$ :  $t = \eta T$ .

In the following analysis, we assume the loss function  $L(\theta)$  can always be reduced to the second order Taylor approximation 1 near critical points. The second order Taylor approximation is common (Mandt et al., 2017) and mild. Particularly, we focus on the behaviors near critical points, which dominates deep learning dynamics. We use g and H to denote the gradient and the Hessian of the loss function, respectively.

**Assumption 1.** The loss function around the critical point c can be approximately written as

$$L(\theta) = L(c) + g(c)(\theta - c) + \frac{1}{2}(\theta - c)^{\top}H(c)(\theta - c).$$

The gradient variance dominates the gradient expectation near critical points. Then we have

$$D(\theta) = \frac{\eta C(\theta)}{2} \approx \frac{\eta}{2B} \left[ \frac{1}{N} \sum_{j=1}^{N} \nabla L(\theta, z_j) \nabla L(\theta, z_j)^{\top} \right] = \frac{\eta}{2B} \text{Fisher}(\theta) \approx \frac{\eta}{2B} [H(\theta)]^{+} \quad (5)$$

near critical points c, where Fisher( $\theta$ ) is the Fisher Information matrix. We use  $[\cdot]^+$  to denote the positive semidefinite transformation of a symmetric matrix: if  $H = U^{\top} \operatorname{diag}(H_1, \dots, H_{n-1}, H_n)U$ , then  $[H]^+ = U^{\top} \operatorname{diag}(|H_1|, \dots, |H_{n-1}|, |H_n|)U$ . The dimension of  $\theta$  is n. The i-th column vector of U is the eigenvector of H corresponding to the eigenvalue  $H_i$ . Equation 5 is also proposed by Jastrzębski et al. (2017); Zhu et al. (2019) and verified by Xie et al. (2020). Daneshmand et al. (2018) also empirically verified that stochastic gradient noise variance is proportional to the magnitude of the corresponding eigenvalues. We present rich empirical evidence in Figure 1 showing that even not near critical points, Equation 5 still holds along the directions of small-magnitude eigenvalues of the Hessian. Please refer to Appendix  $\mathbb C$  for details.

#### 2 SGD Diffusion near Saddle Points

In this section, we demonstrate SGD diffusion in terms of saddle-point escaping. We particularly reveal how hyperparameters affect learning dynamics near saddle points. We focus on learning dynamics near saddle points, as saddle-point escaping is one of the main challenges for accelerating training. If we apply the second order Taylor approximation of the loss, we will have the approximation assumption 2 based on Equation 5, which is empirically verified in Appendix C.

**Assumption 2** (Locally Stable Diffusion Approximation). The diffusion matrix D is position-independent near critical points.

**Theorem 2.1** (SGD Escapes Saddle Points). Suppose c is a critical point, Assumption 1 and 2 hold, the dynamics is governed by Equation 2 with the diffusion matrix D, and the initial parameter is at the saddle point  $\theta = c$ . Then the probability density function of  $\theta$  after time t is given by the Gaussian distribution  $\theta \sim \mathcal{N}(c, \Sigma(t))$ , where  $\Sigma(t) = U^{\top} \operatorname{diag}(\sigma_1^2, \cdots, \sigma_{n-1}^2, \sigma_n^2)U$  and

$$\sigma_i^2(t) = \frac{D_i}{H_i} [1 - \exp(-2H_i t)],$$

where  $D_i$  is the i-th eigenvalue of the diffusion matrix D and  $H_i$  is the i-th eigenvalue of the Hessian matrix H at c. The column vectors of U is exactly the eigenvectors of H. The dynamical time  $t = \eta T$ . In terms of SGD notations, it can be written as

$$\sigma_i^2(T) = \operatorname{sign}(H_i) \frac{\eta}{2R} [1 - \exp(-2H_i \eta T)],$$

where  $\eta$  is the learning rate, B is the batch size, and T is the number of iterations. When  $|H_i|\eta T \ll 1$ , we have the second order Taylor approximation of  $\sigma$  as

$$\sigma_i^2(T) = \frac{|H_i|\eta^2 T}{B} + \mathcal{O}(B^{-1}H_i^2\eta^3 T^2).$$

We leave the proof in Appendix A.1. If  $H_i > 0$ , the *i*-th dimensional distribution quickly converge to a Gaussian distribution,  $\mathcal{N}\left(c_i, \frac{\eta}{2B}\right)$ . If  $H_i < 0$ , the *i*-th dimensional distribution is a Gaussian distribution with the variance exponentially increasing with time t.

# 3 Analysis of Momentum and Adam Diffusion

In this section, we separately study the effects of Momentum and Adaptive Learning Rate in terms of saddle-point escaping and minima selection.

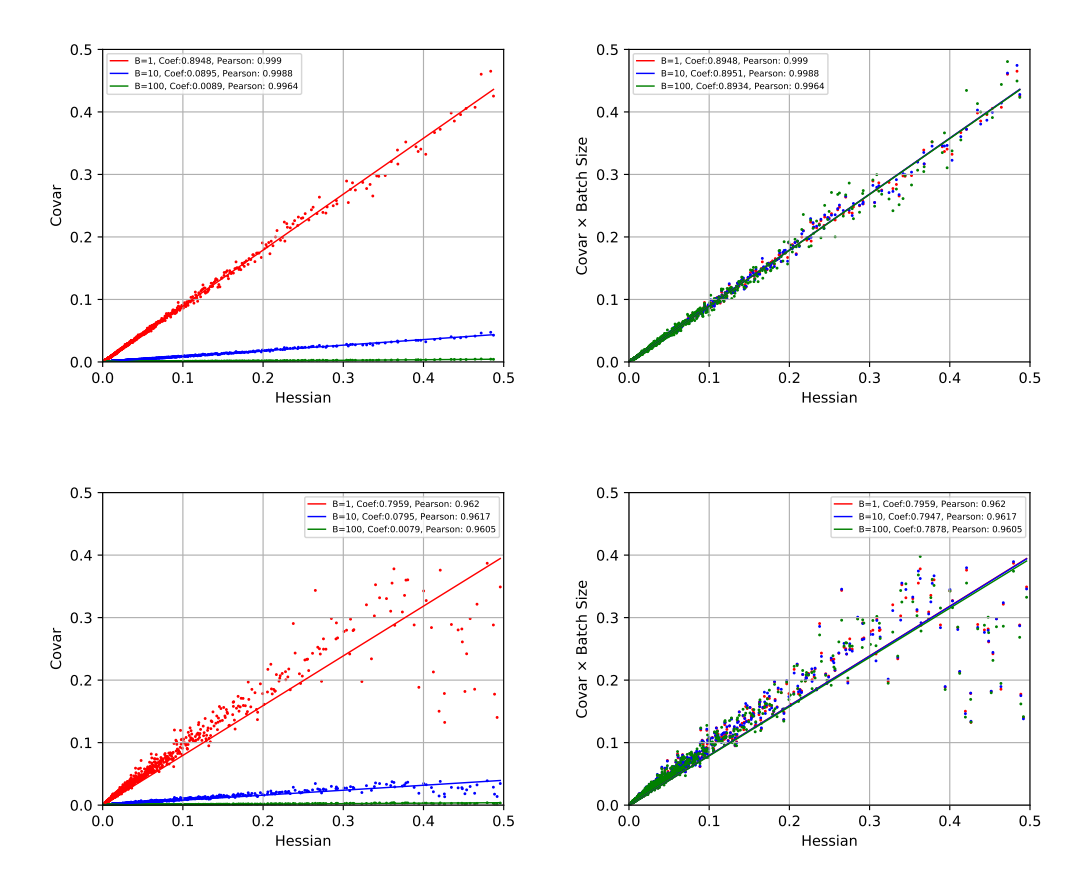


Figure 1: We validate Equation 5 by using three-layer fully-connected network on MNIST (LeCun, 1998). Top Row: Pretrained Models. Bottom Row: Randomly Initialized Models. We display all elements  $H_{(i,j)} \in [1e-4,0.5]$  of the Hessian matrix and the corresponding elements  $C_{(i,j)}$  of gradient covariance matrix in the space spanned by the eigenvectors of Hessian. Even if the model is far from critical points, stochastic gradient noise covariance is still approximately proportional to the Hessian and inverse to the batch size B. The correlation is especially high along the directions with small-magnitude eigenvalues of the Hessian. Small-magnitude eigenvalues of the Hessian indicate the flat directions which we care most in saddle-point escaping.

#### 3.1 Momentum

How does Momentum affect learning dynamics? We note there are two kinds of common momentum implementation, which are, respectively, the cumulative style (Polyak, 1964) in SGD with Momentum and the exponentially moving average in Adam. We first use Adam-style Momentum in our analysis, which is written as

$$\begin{cases}
 m_t = \beta_1 m_{t-1} + (1 - \beta_1) g_t \\
 \theta_t = \theta_{t-1} - \eta m_t,
\end{cases}$$
(6)

where  $\beta_1$  is the momentum hyperparameter. We also write the motion equation in physics with the mass M and the damping coefficient  $\gamma$  as

$$\begin{cases}
r_t = (1 - \gamma dt)r_{t-1} + \frac{F}{M}dt \\
\theta_t = \theta_{t-1} + r_t dt,
\end{cases}$$
(7)

where  $r_t = -m_t$ ,  $F = g_t$ ,  $dt = \eta$ ,  $1 - \gamma dt = \beta_1$ , and  $\frac{dt}{M} = 1 - \beta_1$ . Thus we obtain the continuous-time Momentum dynamics as

$$M\ddot{\theta} = -\gamma M\dot{\theta} + F. \tag{8}$$

The first term as the inertia force is equal to the mass M times the accelerated velocity  $\ddot{\theta}$ , the second term as the damping force is equal to the damping coefficient  $\gamma$  times the physical momentum  $M\dot{\theta}$ , and the third term is equal to the external force F. We can easily obtain the mass  $M = \frac{\eta}{1-\beta_1}$  and the damping coefficient  $\gamma = \frac{1-\beta_1}{\eta}$ . The SGD-style Momentum updating rule is based on  $m_t = \beta_1 m_{t-1} + g_t$  and  $\theta_t = \theta_{t-1} - \eta m_t$ .

The SGD-style Momentum updating rule is based on  $m_t = \beta_1 m_{t-1} + g_t$  and  $\theta_t = \theta_{t-1} - \eta m_t$ . So its dynamics is the same as Equation 8, with the mass  $M = \eta$  and the damping coefficient  $\gamma = \frac{1-\beta_1}{n}$ .

We introduce the gradient expectation and gradient noise into F, and obtain

$$Md\dot{\theta} = -\gamma Md\theta - \frac{\partial L(\theta)}{\partial \theta} dt + [2D(\theta)]^{\frac{1}{2}} dW_t.$$
 (9)

Under Assumption 2, the associated Fokker-Planck Equation in the phase space  $(\theta - \dot{\theta} \text{ space})$  is

$$\frac{\partial P(\theta, r, t)}{\partial t} = -r \cdot \nabla_{\theta} P(\theta, r, t) + \nabla_{\theta} L(\theta) \cdot M^{-1} \nabla_{r} P(\theta, r, t) 
+ \nabla_{r} \cdot M^{-2} D(\theta) \cdot P_{eq}(r) \nabla_{r} [P_{eq}(r)^{-1} P(\theta, r, t)],$$
(10)

where the coordinate  $r = \dot{\theta}$ ,  $P_{eq}(r) = (2\pi)^{-\frac{n}{2}} \det(\beta M)^{\frac{1}{2}} \exp(-\frac{\beta M r^2}{2})$ , and the inverse temperature  $\beta = \gamma M D^{-1}$ . Refer to Zhou (2010); Risken (1996) for details on Equation 10.

**Theorem 3.1** (Momentum Escapes Saddle Points). Suppose c is a critical point, Assumption 1 and 2 hold, the dynamics is governed by Momentum, and the initial parameter is at the saddle point  $\theta = c$ . Then the mean squared displacement near saddle points is

$$\langle \Delta \theta_i^2(t) \rangle = \frac{D_i}{\gamma^3 M^2} [1 - \exp(-\gamma t)]^2 + \frac{D_i}{\gamma M H_i} [1 - \exp(-\frac{2H_i t}{\gamma M})],$$

where  $\Delta\theta(t) = \theta(t) - \theta(0)$  is the displacement of  $\theta$ , and  $\langle \cdot \rangle$  denote the mean value. This first term is the momentum drift effect, and the second term is the diffusion effect. As  $|H_i|\eta T \ll 1$  near ill-conditioned saddle points, it can be written in terms of Adam-style Momentum notations as

$$\langle \Delta \theta_i^2 \rangle = \frac{|H_i|\eta^2}{2(1-\beta_1)B} \left[ 1 - \exp\left(-(1-\beta_1)T\right) \right]^2 + \frac{|H_i|\eta^2 T}{B} + \mathcal{O}(B^{-1}H_i^2\eta^3 T^2),$$

 $and\ in\ terms\ of\ SGD\text{-}style\ Momentum\ notations\ as$ 

$$\langle \Delta \theta_i^2 \rangle = \frac{|H_i|\eta^2}{2(1-\beta_1)^3 B} \left[ 1 - \exp\left(-(1-\beta_1)T\right) \right]^2 + \frac{|H_i|\eta^2 T}{B(1-\beta_1)^2} + \mathcal{O}(B^{-1}H_i^2\eta^3 T^2).$$

We leave the proof in Appendix A.2. We can easily see that both SGD-style Momentum and Adam-style Momentum provide additional momentum drift for passing through saddle points. But Adam-style Momentum does not rescale the diffusion term like SGD-style Momentum. A physics work (Kalinay and Percus, 2012) proves that the phase-space Fokker-Planck Equation 10 can be reduced to a space-dependent Smoluchowski-like equation, which is extended by an effective diffusion correction:

$$\hat{D}_i(\theta) = D_i(\theta) \frac{1 - \sqrt{1 - \frac{4H_i(\theta)}{\gamma^2 M}}}{\frac{2H_i(\theta)}{\gamma^2 M}}.$$
(11)

Based on Theorem 3.2 (SGD Escapes Minima) in Xie et al. (2020) and the effective diffusion correction in (Kalinay and Percus, 2012), we formulate how Momentum escapes minima as Theorem 3.2. Suppose the process of escaping from a given Loss Valley a, the saddle point b is the exit of Loss Valley a, and  $\Delta L = L(b) - L(a)$  is the loss barrier height of the loss valley.

**Theorem 3.2** (Momentum Escapes Minima). Suppose Quasi-Equilibrium Assumption and Low Temperature Assumption of Xie et al. (2020) hold, Assumption 1 and 2 hold, and the dynamics is governed by Momentum. Then the mean escape time from Loss Valley a to the outside of Loss Valley a is given by

$$\tau = \pi \left[ \sqrt{1 + \frac{4|H_{be}|}{\gamma^2 M}} + 1 \right] \frac{1}{|H_{be}|} \exp \left[ \frac{2\gamma M B \Delta L}{\eta} \left( \frac{s}{H_{ae}} + \frac{(1-s)}{|H_{be}|} \right) \right],$$

where the subscription e indicates the escape direction,  $s \in (0,1)$  is a path-dependent parameter, and  $H_{ae}$  and  $H_{be}$  are the eigenvalues of Hessians of the loss function at the minimum a and the saddle point b along the escape direction.

In terms of Adam-style Momentum, it is given by

$$\tau = \pi \left[ \sqrt{1 + \frac{4\eta |H_{be}|}{1 - \beta_1}} + 1 \right] \frac{1}{|H_{be}|} \exp \left[ \frac{2B\Delta L}{\eta} \left( \frac{s}{H_{ae}} + \frac{(1 - s)}{|H_{be}|} \right) \right].$$

In terms of SGD-style Momentum, it is given by

$$\tau = \pi \left[ \sqrt{1 + \frac{4\eta |H_{be}|}{(1 - \beta_1)^2}} + 1 \right] \frac{1}{|H_{be}|} \exp \left[ \frac{2(1 - \beta_1)B\Delta L}{\eta} \left( \frac{s}{H_{ae}} + \frac{(1 - s)}{|H_{be}|} \right) \right].$$

When  $\frac{4|H_{be}|}{\gamma^2 M} \ll 1$ , it is reduced to SGD.

We leave the proof in Appendix A.3. We note that the diffusion theoretical framework relies on another two mild approximation assumptions: Quasi-Equilibrium Approximation and Low Temperature Approximation. In Appendix B, we review why they are common and justified in various kinds of escape problems (Van Kampen, 1992; Jastrzębski et al., 2017).

**Assumption 3** (Quasi-Equilibrium Approximation). The system is in quasi-equilibrium near minima,  $\frac{\partial P(\theta,t)}{\partial t} = -\nabla \cdot J(\theta,t) \approx 0$ .

**Assumption 4** (Low Temperature Approximation). The system is under low temperature (small gradient noise),  $\frac{D_e}{\gamma M} \ll \Delta L_{ab}$ .

#### Algorithm 1: Adam

# $$\begin{split} g_t &= \nabla \hat{L}(\theta_{t-1}); \\ m_t &= \beta_1 m_{t-1} + (1 - \beta_1) g_t; \\ v_t &= \beta_2 v_{t-1} + (1 - \beta_2) g_t^2; \\ \hat{m}_t &= \frac{m_t}{1 - \beta_t^4}; \\ \hat{v}_t &= \frac{v_t}{1 - \beta_2^t}; \\ \theta_t &= \theta_{t-1} - \frac{\eta}{\sqrt{\hat{v}_t} + \epsilon} \hat{m}_t; \end{split}$$

#### Algorithm 2: Adai

$$\begin{split} g_t &= \nabla \hat{L}(\theta_{t-1}); \\ v_t &= \beta_2 v_{t-1} + (1 - \beta_2) g_t^2; \\ \hat{v}_t &= \frac{v_t}{1 - \beta_2^t}; \\ \bar{v}_t &= mean(\hat{v}_t); \\ \mu_t &= (1 - \frac{\beta_0}{\bar{v}_t} \hat{v}_t).Clip(0, 1 - \epsilon); \\ m_t &= \mu_t m_{t-1} + (1 - \mu_t) g_t; \\ \hat{m}_t &= \frac{m_t}{1 - \prod_{z=1}^t \mu_z}; \\ \theta_t &= \theta_{t-1} - \eta \hat{m}_t; \end{split}$$

The previous theoretical results naturally point us a good way to get over saddle points with ill-conditioned Hessians: adaptively adjust learning rates for different parameter,  $\eta_i \propto |H_i|^{-\frac{1}{2}}$ . This is how Adam works. Adam dynamics is written in Algorithm 1. It is easy to see that  $\operatorname{diag}(v_1(\theta),\cdots,v_n(\theta))$  is to estimate the diagonal approximation of the covariance  $C(\theta) = \mathbb{E}[g^\top g]$ , where C is approximately proportional to  $[H]^+$  near critical points. We use Assumption 5 in the following theoretical analysis.

**Assumption 5** (Ideally Adaptive Approximation). The practical adaptive matrix  $V^{-\frac{1}{2}}$  is approximately equivalent to the ideal adaptive matrix  $C^{-\frac{1}{2}}$  for learning dynamics.

The continuous-time dynamics of Adam can also be written as Equation 8, except that the mass  $M=\frac{\hat{\eta}}{1-\beta_1}$ , and the damping coefficient  $\gamma=\frac{1-\beta_1}{\hat{\eta}}$ . We emphasize that learning rate is not a real number but a matrix in Adam, and is the diagonal approximation of the ideal learning rate matrix  $\hat{\eta}=\eta C^{-\frac{1}{2}}$  in practice, where  $C^{-\frac{1}{2}}$  is also called a preconditioning matrix. We need apply the adaptive time continuation  $d\hat{t}_i=\hat{\eta}_i$  in *i*-th dimension. We define  $\hat{t}_i$  of T iterations as the sum of  $\hat{\eta}_i$  of each iteration. Thus the Fokker-Planck Equation associated with Adam dynamics can still be written as Equation 10.

**Proposition 1** (Adam Escape Saddle Points). Suppose c is a critical point, Assumption 1, 2, and 5 hold, the dynamics is governed by Adam, and the initial parameter is at the saddle point  $\theta = c$ . Then the mean squared displacement is written as

$$\langle \Delta \theta_i^2(\hat{t}_i) \rangle = \frac{D_i}{\gamma^2 M} [1 - \exp(-\gamma \hat{t}_i)]^2 + \frac{D_i}{\gamma M H_i} [1 - \exp(-\frac{2H_i \hat{t}_i}{\gamma M})].$$

This first term is the momentum term, and the second term is the diffusion term. Under  $|H_i|\eta T \ll 1$ , it can be respectively written in terms of Adam notations as:

$$\langle \Delta \theta_i^2 \rangle = \frac{\eta^2}{2(1-\beta_1)} \left[ 1 - \exp\left( -(1-\beta_1)T \right) \right]^2 + \eta^2 T + \mathcal{O}(\sqrt{B|H_i|}\eta^3 T^2).$$

The proof is complete by Theorem 3.1 and Assumption 5. We can obtain rich information about Adam in Proposition 1. Adam escapes from saddle points fast, because both the momentum drift and the diffusion effect are Hessian-independent near saddle points. The advantage of Adam over RMSprop comes from the additional momentum drift effect. Theorem 3.1 and Proposition 1 together have theoretically demonstrate the different effects of Adaptive Learning Rate and Momentum.

**Proposition 2** (Adam Escapes Minima). Adam cannot learn flat minima as well as SGD, as the mean escape time of Adam only exponentially depends on the squared root of eigenvalues of the Hessian at minima:

$$\tau = \pi \left[ \sqrt{1 + \frac{4\eta \sqrt{B|H_{be}|}}{1 - \beta_1}} + 1 \right] \frac{|\det(H_a^{-1}H_b)|^{\frac{1}{4}}}{|H_{be}|} \exp\left[ \frac{2\sqrt{B}\Delta L}{\eta} \left( \frac{s}{\sqrt{H_{ae}}} + \frac{(1 - s)}{\sqrt{|H_{be}|}} \right) \right],$$

where  $\tau$  is the mean escape time.

The proof is based on Theorem 3.2 and Assumption 5, seen in Appendix A.4. Proposition 2 demonstrates that Adam cannot learn flat minima as well as SGD, as the Adam dynamics of escaping sharp minima is less sensitive to the minima sharpness than SGD. The minima sharpness is mainly reflected by  $H_{ae}$ . The weaker Hessian-dependent diffusion term damages flat minima selection. In summary, Adam is better at saddle-point escaping but worse at flat minima selection.

#### 4 Adaptive Inertia

Theorem 3.1 and 3.2 naturally leads to the idea that parameter-wisely adaptive inertia can achieve the approximately Hessian-independent momentum drift without damaging flat minima selection. In this section, we give up Adaptive Learning Rate and propose a novel adaptive mechanism: Adaptive Inertia. The total momentum drift effect during passing a saddle point is given by

$$\langle \Delta \theta_i \rangle^2 = \frac{|H_i|\eta^2}{2(1-\beta_1)B}.\tag{12}$$

Adaptive Inertia Estimation (Adai) is displayed in Algorithm 2. To make the optimizer more robust, we apply the normalization by  $mean(\hat{v}_t)$ , the mean of all elements in  $\hat{v}_t$ . We note that SGD-style Momentum does not work well in Adai, as it seriously damages flat minima selection based on Theorem 3.2.

In Adai,  $I-\mu$  indicates the adaptive inertia matrix. The ideal adaptive updating is to keep  $I-\mu=\frac{n\beta_0}{\|V\|_1}V$ , where  $\|\cdot\|_1$  is the trace norm. We note that V is the diagonal approximation of C, where  $\frac{\|V\|_1}{n}$  is exactly the estimated expectation of gradient variance of all dimensions. The default setting of  $\beta_0$  and  $\beta_2$  are respectively 0.1 and 0.99. The bound hyperparameter  $\epsilon$  is to keep  $\mu_i \in [0, 1-\epsilon]$ , which avoids extremely large inertia. The default setting  $\epsilon=0.001$  means the maximal inertia is 1000 times the minimal inertia, as  $M=\eta(1-\beta_1)^{-1}$ . We replace  $\beta_1$  of Adam by  $\beta_0$ , so Adai does not increase the number of hyperparameters. Moreover, the computational cost of Adai is nearly the same as Adam. We do not observe a noticeable time cost difference in practice.

The Fokker-Planck Equation associated with Adai dynamics in the phase space can be written as Equation 10, except that we need replace the mass coefficient and the damping coefficient by the mass matrix and the damping matrix:  $M = \eta(I - \mu)^{-1}$  and  $\gamma = \eta^{-1}(I - \mu)$ .

**Proposition 3** (Adai Escapes Saddle Points). Suppose c is a critical point, Assumption 1, 2, and 5 hold, the dynamics is governed by SGD with Momentum, and the initial parameter is at the saddle point  $\theta = c$ . Then the total momentum drift in the procedure of passing through the saddle point is given by

$$\langle \Delta \theta_i \rangle^2 = \frac{\|V\|_1 \eta^2}{\beta_0 n} = \frac{\sum_{i=1}^n |H_i| \eta^2}{\beta_0 nB},$$

where  $\sum_{i=1}^{n} |H_i|$  is the sum of the absolute values of the eigenvalues of the Hessian at c.

Proposition 3 shows that Adai can escape saddle points efficiently due to the Hessian-independent momentum drift. In early epochs of training ResNet18 on CIFAR-10, the momentum drift effect of Adai is observed to dominate Adam by nearly 1000 times. But this domination depends on tasks. We do not rigorously claim that Adai must converge faster than or as fast as Adam, because they have essentially different theoretical mechanisms. We will empirically compare Adai and Adam instead.

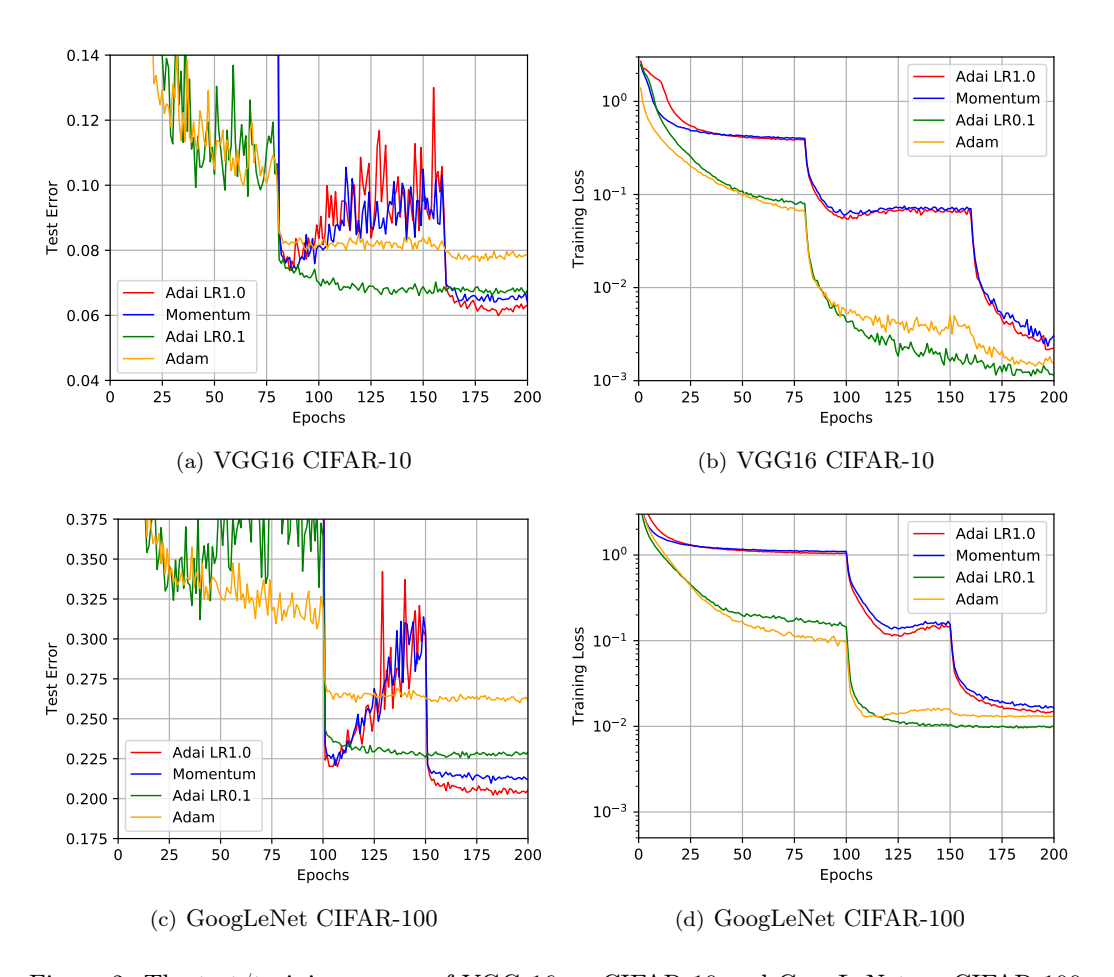


Figure 2: The test/training curves of VGG-16 on CIFAR-10 and GoogLeNet on CIFAR-100.

**Proposition 4** (Adai Escapes Minima). Adai can learn flat minima better than Adam, as the mean escape time of Adai exponentially depends on eigenvalues of the Hessian at minima:

$$\tau = \pi \left[ \sqrt{1 + \frac{4\eta \sum_{i=1}^{n} |H_{bi}|}{\beta_0 n}} + 1 \right] \frac{1}{|H_{be}|} \exp \left[ \frac{2B\Delta L}{\eta} \left( \frac{s}{H_{ae}} + \frac{(1-s)}{|H_{be}|} \right) \right],$$

where  $\tau$  is the mean escape time.

We leave the proof in Appendix A.5. By Proposition 4, we know Adai does not affect the exponential relation between the mean escape time and the Hessian at minima. We note  $\mathbb{E}[|H_{be}|] > \mathbb{E}\left[\frac{\sum_{i=1}^{n}|H_{bi}|}{n}\right]$ , because the escape directions are more likely to be the sharp directions. Thus another hidden advantage of Adai is slightly accelerating escaping minima. By Theorem 3.2 and Proposition 4, Adai favors flat minima as much as SGD, and search more minima than SGD given a limited time. The second point leads to a slight generalization advantage over SGD.

## 5 Empirical Analysis

Experiment 1. Generalization and Convergence Speed. We conduct the main experiment to compare Adai with Adam and SGD with Momentum in terms of convergence speed and generalization.

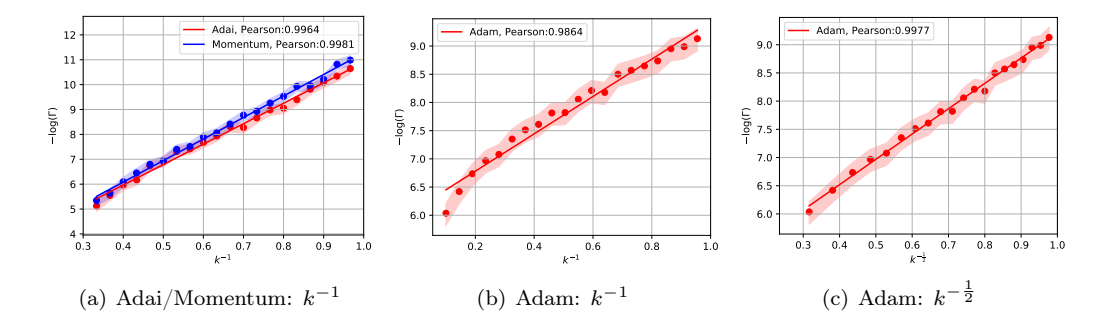


Figure 3: Flat Minima Selection:  $Adai \approx Momentum \gg Adam$ . We display the number of iterations for escaping the given loss valley to the relative minima flatness indicated by the rescaling factor  $k^{-1}$ . We repeat each simulation for 100 runs. The log-scale expected number of iterations  $-\log(\Gamma)$  with the 95% confidence interval is displayed. Adam is significantly less sensitive to the minima sharpness than both Momentum and Adai. As we predict,  $-\log(\Gamma)$  is approximately linear with  $k^{-1}$  for Momentum and Adai, while  $-\log(\Gamma)$  is only approximately linear with  $k^{-\frac{1}{2}}$  for Adam. Although Adai and Momentum favor flat minima similarly, Adai can escape loss valleys even slightly fast than Momentum as we predicted.

Datasets: CIFAR-10, CIFAR-100 (Krizhevsky et al., 2009), and ImageNet(ILSVRC2012) (Deng et al., 2009). Models: ResNet (He et al., 2016), VGG (Simonyan and Zisserman, 2014), DenseNet (Huang et al., 2017), and GoogLeNet (Szegedy et al., 2015). The hyperparameter settings can be found in Appendix D.

We display the test performance of all models in Table 1. We display the optimal training/test curves of VGG-16 and GoogLeNet in Figure 2. We have empirically verified that (1) stochastic gradient noise is Gaussian, and (2) the gradient covariance matrix is approximately proportional to the Hessian and inverse to the batch size, seen in Appendix C. In Appendix D, we further present (3) the figures of other models, and (4) the convergence comparison in 1000 epochs.

Adai generalizes significantly better than Adam, while they converge similarly fast. Adai even generalizes better than SGD with Momentum, while they converge similarly fast. We also notice that Adai usually converges in a lower training loss than Adam and SGD with Momentum, respectively, with a similar convergence speed. We note that Adai with  $\eta=1$  "happen to" have a similarly fast convergence speed as Momentum with  $\eta=0.1$ . This is not coincidence. In case of  $\beta_1=0.9,\ m_t\approx\mathbb{E}[g_t]$  in Adam-style Momentum, while  $m_t\approx10\mathbb{E}[g_t]$  in SGD-style Momentum.

It is not surprising that larger initial learning rates lead to better generalization in our experiments, which is also reported by He et al. (2019); Li et al. (2019). Our theoretical results provide another explanation: given the realistic computational time, the optimizers with large learning rates can search more flat minima.

Experiment 2. The Mean Escape Time Analysis. We empirically study how the escape rate  $\Gamma$ , which equals to the inverse mean escape time, depends on the minima sharpness for different optimizers in Figure 3. Our method for adjusting the minima sharpness is to multiply a rescaling factor  $\sqrt{k}$  to each parameter, and the Hessian will be proportionally rescaled by a factor k. If we let  $L(\theta) = f(\theta) \to L(\theta) = f(\sqrt{k}\theta)$ , then  $H(\theta) = \nabla^2 f(\theta) \to H(\theta) = k\nabla^2 f(\theta)$ . Thus, we can use k to indicate the relative minima sharpness. Both the theoretical result and the empirical result support that Adam is significantly less sensitive to the minima sharpness than both Momentum and Adai. We also notice that, Adai escapes loss valleys slight faster than Momentum.

**Test Function:** We use Styblinski-Tang Function, which a commonly used function in nonconvex optimization, as the loss function, so we clearly know the boundary between loss valleys. **Setting:** We leave more details in Appendix E.

#### 6 Conclusion

Adam can achieve approximately Hessian-independent drift and diffusion near saddle points, which accelerates saddle-point escaping efficiently. But its Hessian-independent diffusion effect seriously damages flat minima selection. We propose a novel optimizer Adai which uses parameter-wisely adaptive inertia. Adai can provide a Hessian-independent momentum drift effect to accelerate training, and almost does not affect the diffusion effect term. Thus Adai can theoretically accelerate training and favor flat minima well at the same time. Our empirical analysis demonstrates that, with similar convergence speed, Adai generalizes better than Adam and SGD, respectively. It fully supports that Adai can be a promising alternative to both Adam and SGD.

#### Acknowledgement

MS was supported by the International Research Center for Neurointelligence (WPI-IRCN) at The University of Tokyo Institutes for Advanced Study.

#### References

- Achille, A. and Soatto, S. (2019). Where is the information in a deep neural network? arXiv preprint arXiv:1905.12213.
- Chen, J. and Gu, Q. (2018). Closing the generalization gap of adaptive gradient methods in training deep neural networks. arXiv preprint arXiv:1806.06763.
- Daneshmand, H., Kohler, J., Lucchi, A., and Hofmann, T. (2018). Escaping saddles with stochastic gradients. In *International Conference on Machine Learning*, pages 1155–1164.
- Deng, J., Dong, W., Socher, R., Li, L.-J., Li, K., and Fei-Fei, L. (2009). Imagenet: A large-scale hierarchical image database. In 2009 IEEE conference on computer vision and pattern recognition, pages 248–255. Ieee.
- Duchi, J., Hazan, E., and Singer, Y. (2011). Adaptive subgradient methods for online learning and stochastic optimization. *Journal of machine learning research*, 12(Jul):2121–2159.
- Gnedenko, B., Kolmogorov, A., Gnedenko, B., and Kolmogorov, A. (1954). Limit distributions for sums of independent. *Am. J. Math*, 105.
- He, F., Liu, T., and Tao, D. (2019). Control batch size and learning rate to generalize well: Theoretical and empirical evidence. In Advances in Neural Information Processing Systems, pages 1141–1150.
- He, K., Zhang, X., Ren, S., and Sun, J. (2016). Deep residual learning for image recognition. In *Proceedings of the IEEE conference on computer vision and pattern recognition*, pages 770–778.
- Hinton, G., Srivastava, N., and Swersky, K. (2012). Neural networks for machine learning lecture 6a overview of mini-batch gradient descent.
- Hu, W., Li, C. J., Li, L., and Liu, J.-G. (2019). On the diffusion approximation of nonconvex stochastic gradient descent. *Annals of Mathematical Sciences and Applications*, 4(1):3–32.
- Huang, G., Liu, Z., Van Der Maaten, L., and Weinberger, K. Q. (2017). Densely connected convolutional networks. In *Proceedings of the IEEE conference on computer vision and* pattern recognition, pages 4700–4708.

- Jastrzębski, S., Kenton, Z., Arpit, D., Ballas, N., Fischer, A., Bengio, Y., and Storkey, A. (2017). Three factors influencing minima in sgd. arXiv preprint arXiv:1711.04623.
- Kalinay, P. and Percus, J. K. (2012). Phase space reduction of the one-dimensional fokker-planck (kramers) equation. *Journal of Statistical Physics*, 148(6):1135–1155.
- Kingma, D. P. and Ba, J. (2015). Adam: A method for stochastic optimization. 3rd International Conference on Learning Representations, ICLR 2015.
- Krizhevsky, A., Hinton, G., et al. (2009). Learning multiple layers of features from tiny images.
- LeCun, Y. (1998). The mnist database of handwritten digits. http://yann. lecun. com/exdb/mnist/.
- Li, Q., Tai, C., et al. (2017). Stochastic modified equations and adaptive stochastic gradient algorithms. In *Proceedings of the 34th International Conference on Machine Learning-Volume 70*, pages 2101–2110. JMLR. org.
- Li, Y., Wei, C., and Ma, T. (2019). Towards explaining the regularization effect of initial large learning rate in training neural networks. In *Advances in Neural Information Processing Systems*, pages 11669–11680.
- Loshchilov, I. and Hutter, F. (2017). Decoupled weight decay regularization. 7th International Conference on Learning Representations, ICLR 2019.
- Luo, L., Xiong, Y., Liu, Y., and Sun, X. (2019). Adaptive gradient methods with dynamic bound of learning rate. 7th International Conference on Learning Representations, ICLR 2019.
- Mandt, S., Hoffman, M. D., and Blei, D. M. (2017). Stochastic gradient descent as approximate bayesian inference. *The Journal of Machine Learning Research*, 18(1):4873–4907.
- Polyak, B. T. (1964). Some methods of speeding up the convergence of iteration methods. USSR Computational Mathematics and Mathematical Physics, 4(5):1–17.
- Raginsky, M., Rakhlin, A., and Telgarsky, M. (2017). Non-convex learning via stochastic gradient langevin dynamics: a nonasymptotic analysis. In *Conference on Learning Theory*, pages 1674–1703.
- Reddi, S. J., Kale, S., and Kumar, S. (2019). On the convergence of adam and beyond. 6th International Conference on Learning Representations, ICLR 2018.
- Risken, H. (1996). Fokker-planck equation. In *The Fokker-Planck Equation*, pages 63–95. Springer.
- Sato, I. and Nakagawa, H. (2014). Approximation analysis of stochastic gradient langevin dynamics by using fokker-planck equation and ito process. In *International Conference on Machine Learning*, pages 982–990.
- Simonyan, K. and Zisserman, A. (2014). Very deep convolutional networks for large-scale image recognition. arXiv preprint arXiv:1409.1556.
- Simsekli, U., Sagun, L., and Gurbuzbalaban, M. (2019). A tail-index analysis of stochastic gradient noise in deep neural networks. In *International Conference on Machine Learning*, pages 5827–5837.
- Szegedy, C., Liu, W., Jia, Y., Sermanet, P., Reed, S., Anguelov, D., Erhan, D., Vanhoucke, V., and Rabinovich, A. (2015). Going deeper with convolutions. In *Proceedings of the IEEE conference on computer vision and pattern recognition*, pages 1–9.

- Van Kampen, N. G. (1992). Stochastic processes in physics and chemistry, volume 1. Elsevier.
- Wilson, A. C., Roelofs, R., Stern, M., Srebro, N., and Recht, B. (2017). The marginal value of adaptive gradient methods in machine learning. In Advances in Neural Information Processing Systems, pages 4148–4158.
- Xie, Z., Sato, I., and Sugiyama, M. (2020). A diffusion theory for minima selection: Stochastic gradient descent escapes from sharp minima exponentially fast. arXiv preprint arXiv:2002.03495.
- Xu, P., Chen, J., Zou, D., and Gu, Q. (2018). Global convergence of langevin dynamics based algorithms for nonconvex optimization. In Advances in Neural Information Processing Systems, pages 3122–3133.
- Zaheer, M., Reddi, S., Sachan, D., Kale, S., and Kumar, S. (2018). Adaptive methods for nonconvex optimization. In Advances in neural information processing systems, pages 9793–9803.
- Zeiler, M. D. (2012). Adadelta: an adaptive learning rate method. arXiv preprint arXiv:1212.5701.
- Zhang, Y., Liang, P., and Charikar, M. (2017). A hitting time analysis of stochastic gradient langevin dynamics. In *Conference on Learning Theory*, pages 1980–2022.
- Zhou, H.-X. (2010). Rate theories for biologists. Quarterly reviews of biophysics, 43(2):219–293.
- Zhu, Z., Wu, J., Yu, B., Wu, L., and Ma, J. (2019). The anisotropic noise in stochastic gradient descent: Its behavior of escaping from sharp minima and regularization effects.

#### A Proofs

#### A.1 Proof of Theorem 2.1

*Proof.* It is easy to validate that the probability density function

$$P(\theta, t) = \frac{1}{\sqrt{(2\pi)^k \det(\Sigma(t))}} \exp\left(-\frac{1}{2}(\theta - c)^{\top} \Sigma(t)(\theta - c)\right)$$
(13)

is the solution of the Fokker-Planck Equation 4. Without losing generality, we only validate one-dimensional solution, such as Dimension i.

The first term in Equation 4 can be written as

$$\frac{\partial P(\theta, t)}{\partial t} = -\frac{1}{2} \frac{1}{\sqrt{2\pi\sigma^2}} \frac{1}{\sigma^2} \exp\left(-\frac{\theta^2}{2\sigma^2}\right) \frac{\partial \sigma^2}{\partial t} + \frac{1}{\sqrt{2\pi\sigma^2}} \exp\left(-\frac{\theta^2}{2\sigma^2}\right) \frac{\theta^2}{2\sigma^4} \frac{\partial \sigma^2}{\partial t}$$
(14)

$$= \frac{1}{2} \left( \frac{\theta^2}{\sigma^4} - \frac{1}{\sigma^2} \right) P(\theta, t) \frac{\partial \sigma^2}{\partial t}. \tag{15}$$

The second term in Equation 4 can be written as

$$\nabla \cdot [P(\theta, t)\nabla L(\theta)] = P(\theta)H + H\theta \frac{1}{\sqrt{2\pi\sigma^2}} \exp\left(-\frac{\theta^2}{2\sigma^2}\right) \left(-\frac{\theta}{\sigma^2}\right)$$
(16)

$$=H\left(1-\frac{\theta^2}{\sigma^2}\right)P(\theta,t). \tag{17}$$

The third term in Equation 4 can be written as

$$D\nabla^2 P(\theta, t) = -D \frac{\sigma^2 - \theta^2}{\sigma^5 \sqrt{2\pi}} \exp\left(-\frac{\theta^2}{2\sigma^2}\right)$$
 (18)

$$= D\left(\frac{\theta^2}{\sigma^4} - \frac{1}{\sigma^2}\right) P(\theta, t). \tag{19}$$

By Term1 = Term2 + Term3, we have

$$\frac{1}{2}(\theta^2 - \sigma^2)\frac{\partial \sigma^2}{\partial t} = H\sigma^2(\sigma^2 - \theta^2) + D(\theta^2 - \sigma^2)$$
(20)

$$\frac{\partial \sigma^2}{\partial t} = 2D - 2H\sigma^2. \tag{21}$$

The initial condition of  $\sigma^2$  is given by  $\sigma^2(0) = 0$ . We can validate that  $\sigma^2$  satisfies

$$\sigma_i^2(t) = \frac{D_i}{H_i} [1 - \exp(-2H_i t)]. \tag{22}$$

It is true along all eigenvectors' directions.

By  $D = \frac{\eta}{2B}H$ , we can get the results of SGD diffusion:

$$\sigma_i^2(T) = \operatorname{sign}(H_i) \frac{\eta}{2B} [1 - \exp(-2H_i \eta T)]$$
(23)

#### A.2 Proof of Theorem 3.1

*Proof.* The complete solution of  $\theta$ , r after time t is actually given by the Gaussian distribution

$$P(\theta, r, t) = P_{eq}(r)P(\theta, t),$$

where

$$\begin{cases} P_{eq}(r) = \frac{1}{\sqrt{(2\pi)^k \det(\Sigma_r)}} \exp\left(-\frac{1}{2}r^\top \Sigma_r r\right) \\ P(\theta, t) = \frac{1}{\sqrt{(2\pi)^k \det(\Sigma(t))}} \exp\left(-\frac{1}{2}(\theta - c(t))^\top \Sigma(t)(\theta - c(t))\right) \\ \Sigma_r = U^\top \operatorname{diag}(r_{eq,1}^2, \cdots, r_{eq,n-1}^2, r_{eq,n}^2) U \\ \Sigma(t) = U^\top \operatorname{diag}(\sigma_1^2(t), \cdots, \sigma_{n-1}^2(t), \sigma_n^2(t)) U \\ r_{eq,i}^2 = \frac{D_i}{\gamma M^2} \\ c(t) = c + \frac{r_{eq}}{\gamma} [1 - \exp(-\gamma t)] \\ \sigma_i^2(t) = \frac{2D_i}{\gamma M H_i} [1 - \exp(-\frac{H_i t}{\gamma M})]. \end{cases}$$

To have the proof more concise, we use a math trick to decompose the solution  $P(\theta, r, t) = P(r, t)P(\theta, t)$  into two parts: the velocity solution P(r, t) and the position solution  $P(\theta, t)$ . This is a trick for simplifying dynamical equations, which is widely used in statistical physics. Step I:

The velocity distribution P(r,t) must be the solution of the free diffusion equation in the velocity space. We can approximately ignore the gradient expectation term  $-\frac{\partial L(\theta)}{\partial \theta}$  in dynamical equations near critical points, as the gradient expectation is much smaller the gradient noise scale near critical points. Near critical points, the velocity r obeys the equilibrium distribution

$$P(r,t) \approx P_{eq}(r) = (2\pi)^{-\frac{n}{2}} \det(\beta M)^{\frac{1}{2}} \exp(-\frac{\beta M r^2}{2}),$$
 (24)

where  $\beta = \gamma M D^{-1}$  is the inverse temperature matrix. This is a generalized Boltzmann distribution.

Step II:

Again, we use the same trick to decompose the solution  $P(\theta,t)$  into two parts. The first part is the momentum drift effect, which decides c(t), the center position; the second part is the diffusion effect, which decides  $\Sigma(t)$  as the covariance matrix. The momentum drift effect is governed by the motion equation without random noise, while the diffusion effect is governed by the diffusion equation without conservative force, which is the gradient expectation in deep learning.

Step II (a): the momentum drift effect.

We can write the dynamics of the momentum drift effect as

$$M\ddot{c}(t) = -\gamma M\dot{c}(t). \tag{25}$$

We also have ignored the conservative force -H[c(t)-c(0)] near saddle points, as  $|H_i| \ll \gamma M$  exists for ill-condition Hessian eigenvalues. We focus on the behaviors near ill-conditioned saddle points, where Hessian eigenvalues are small along the escape directions.

The initial condition is given by c(0) = c,  $\dot{c}(0) = r_{eq}$ , and  $\ddot{c}(0) = -\gamma r_{eq}$ . Then we can obtain the solution c(t) as

$$c_i(t) = c_i + \frac{r_{i,eq}}{\gamma} [1 - \exp(-\gamma t)]. \tag{26}$$

Step II (b): the diffusion effect.

We can get the dynamics of the diffusion effect as

$$\gamma M d\theta = -\frac{\partial L(\theta)}{\partial \theta} dt + [2D(\theta)]^{\frac{1}{2}} dW_t. \tag{27}$$

This is equivalent to SGD dynamics with  $\hat{\eta} = \frac{\eta}{\gamma M}$ . The expression of  $P(\theta, t)$  and  $\sigma_i^2(t)$  is directly given by Theorem 2.1 as

$$\sigma_i^2(t) = \frac{D_i}{\gamma M H_i} [1 - \exp(-\frac{2H_i t}{\gamma M})].$$
 (28)

We combine the momentum drift effect and the diffusion effect together, and then obtain the mean squared displacement of  $\theta$  as

$$\langle \Delta \theta_i^2(t) \rangle = (c_i(t) - c_i)^2 + \sigma_i^2(t) = \frac{D_i}{\gamma^3 M^2} [1 - \exp(-\gamma t)]^2 + \frac{D_i}{\gamma M H_i} [1 - \exp(-\frac{2H_i t}{\gamma M})]. \quad (29)$$

We respectively introduce the notations of Adam-style Momentum and SGD-style Momentum, and apply the second order Taylor expansion in case of small  $-\frac{2H_it}{\gamma M}$ . Then we obtain

$$\langle \Delta \theta_i^2 \rangle = \frac{|H_i|\eta^2}{2(1-\beta_1)B} \left[ 1 - \exp\left(-(1-\beta_1)T\right) \right]^2 + \frac{|H_i|\eta^2 T}{B} + \mathcal{O}(B^{-1}H_i^2\eta^3 T^2)$$
 (30)

for Adam-style Momentum, and

$$\langle \Delta \theta_i^2 \rangle = \frac{|H_i|\eta^2}{2(1-\beta_1)^3 B} \left[ 1 - \exp\left(-(1-\beta_1)T\right) \right]^2 + \frac{|H_i|\eta^2 T}{B(1-\beta_1)^2} + \mathcal{O}(B^{-1}H_i^2\eta^3 T^2)$$
(31)

for SGD-style Momentum.

#### A.3 Proof of Theorem 3.2

*Proof.* The proof closely relates to the proof of Theorem 3.2 in Xie et al. (2020) and a physics work (Kalinay and Percus, 2012).

We first discover how SGD dynamics differs from Momentum dynamics in terms of escaping loss valleys. In this approach, we may transform the proof for Theorem 3.2 of Xie et al. (2020) into the proof for Theorem 3.2 with the effective diffusion correction. We use J and j to denote the probability current and the probability flux respectively. According to Gauss Divergence Theorem, we may rewrite the Fokker-Planck Equation 10 as

$$\frac{\partial P(\theta, r, t)}{\partial t} = -r \cdot \nabla_{\theta} P(\theta, r, t) + \nabla_{\theta} L(\theta) \cdot M^{-1} \nabla_{r} P(\theta, r, t) + \nabla_{r} \cdot M^{-2} D(\theta) \cdot P_{eq}(r) \nabla_{r} [P_{eq}(r)^{-1} P(\theta, r, t)]$$
(32)

$$= -\nabla \cdot J(\theta, t). \tag{33}$$

We will take similar forms of the proof in Xie et al. (2020) as follows. The mean escape time is written as

$$\tau = \frac{P(\theta \in V_a)}{\int_{S_a} J \cdot dS}.$$
 (34)

To compute the mean escape time, we decompose the proof into two steps: 1) compute the probability of locating in valley a,  $P(\theta \in V_a)$ , and 2) compute the probability flux  $j = \int_{S_a} J \cdot dS$ . The definition of the probability flux integral may refer to Gauss Divergence Theorem.

Step 1:

Fortunately, the stationary probability distribution inside Valley a in Momentum dynamics is also given by a Gaussian distribution in Theorem 2.1 as

$$\sigma_i^2(t) = \frac{D_i}{\gamma M H_i}. (35)$$

Under Quasi-Equilibrium Assumption, the distribution around minimum a is  $P(\theta) = P(a) \exp\left[-\frac{\gamma M}{2}(\theta-a)^{\top}(D_a^{-\frac{1}{2}}H_aD_a^{-\frac{1}{2}})(\theta-a)\right]$ . We use the T notation as the temperature parameter in the stationary distribution, and use the D notation as the diffusion coefficient in the dynamics, for their different roles.

$$P(\theta \in V_a) \tag{36}$$

$$= \int_{\theta \in V_a} P(\theta) dV \tag{37}$$

$$=P(a)\int_{\theta\in V_a} \exp\left[-\frac{\gamma M}{2}(\theta-a)^{\top} (D_a^{-\frac{1}{2}} H_a D_a^{-\frac{1}{2}})(\theta-a)\right] dV$$
 (38)

$$\approx P(a) \int_{\theta \in (-\infty, +\infty)} \exp\left[-\frac{\gamma M}{2} (\theta - a)^{\top} \left(D_a^{-\frac{1}{2}} H_a D_a^{-\frac{1}{2}}\right) (\theta - a)\right] dV \tag{39}$$

$$=P(a)\frac{(2\pi\gamma M)^{\frac{n}{2}}}{\det(D_a^{-1}H_a)^{\frac{1}{2}}}\tag{40}$$

This result of  $P(\theta \in V_a)$  in Momentum only differs from SGD by the temperature correction  $\gamma M$ .

Step 2: We directly introduce the effective diffusion results from (Kalinay and Percus, 2012) into our analysis. As we only employ the Smoluchowski Equation along the escape direction, we use the one-dimensional expression along the escape direction (an eigenvector direction) for simplicity. Without losing clarity, we use the commonly used T to denote the temperature in the proof.

In case of SGD (Xie et al., 2020), we can obtain Smoluchowski Equation in position space:

$$J = D(\theta) \exp\left(\frac{-L(\theta)}{T}\right) \nabla \left[\exp\left(\frac{L(\theta)}{T}\right) P(\theta)\right],\tag{41}$$

where T = D. According to (Kalinay and Percus, 2012), in case of finite inertia, we can transform the phase-space equation into the position-space Smoluchowski-like form with the effective diffusion correction:

$$J = \hat{D}(\theta) \exp\left(\frac{-L(\theta)}{T}\right) \nabla \left[\exp\left(\frac{L(\theta)}{T}\right) P(\theta)\right], \tag{42}$$

where  $T = \frac{D}{\gamma M}$ , and  $\hat{D}$  defined by Equation 11 replaces standard D. We assume the point s is a midpoint on the most possible path between a and b, where L(s) = (1-s)L(a) + sL(b). The temperature  $T_a$  dominates the path  $a \to s$ , while temperature  $T_b$  dominates the path  $s \to b$ . So we have

$$\nabla \left[ \exp \left( \frac{L(\theta) - L(s)}{T} \right) P(\theta) \right] = J D^{-1} \exp \left( \frac{L(\theta) - L(s)}{T} \right). \tag{43}$$

We integrate the equation from Valley a to the outside of Valley a along the most possible escape path

$$Left = \int_{a}^{c} \frac{\partial}{\partial \theta} \left[ \exp\left(\frac{L(\theta) - L(s)}{T}\right) P(\theta) \right] d\theta \tag{44}$$

$$= \int_{a}^{s} \frac{\partial}{\partial \theta} \left[ \exp \left( \frac{L(\theta) - L(s)}{T_{a}} \right) P(\theta) \right] d\theta \tag{45}$$

$$+ \int_{s}^{c} \frac{\partial}{\partial \theta} \left[ \exp \left( \frac{L(\theta) - L(s)}{T_{b}} \right) P(\theta) \right] d\theta \tag{46}$$

$$= [P(s) - \exp\left(\frac{L(a) - L(s)}{T_a}\right) P(a)] + [0 - P(s)]$$
(47)

$$= -\exp\left(\frac{L(a) - L(s)}{T_a}\right) P(a) \tag{48}$$

$$Right = -J \int_{a}^{c} D^{-1} \exp\left(\frac{L(\theta) - L(s)}{T}\right) d\theta \tag{49}$$

We move J to the outside of integral based on Gauss's Divergence Theorem, because J is fixed on the escape path from one minimum to another. As there is no field source on the escape path,  $\int_V \nabla \cdot J(\theta) dV = 0$  and  $\nabla J(\theta) = 0$ . Obviously, probability sources are all near minima in deep learning. So we obtain

$$J = \frac{\exp\left(\frac{L(a) - L(s)}{T_a}\right) P(a)}{\int_a^c \hat{D}^{-1} \exp\left(\frac{L(\theta) - L(s)}{T}\right) d\theta}.$$
 (50)

Near saddle points, we have

$$\int_{a}^{c} \hat{D}^{-1} \exp\left(\frac{L(\theta) - L(s)}{T}\right) d\theta \tag{51}$$

$$\approx \int_{a}^{c} \hat{D}^{-1} \exp \left[ \frac{L(b) - L(s) + \frac{1}{2}(\theta - b)^{\mathsf{T}} H_{b}(\theta - b)}{T_{b}} \right] d\theta \tag{52}$$

$$\approx \hat{D}_b^{-1} \int_{-\infty}^{+\infty} \exp\left[\frac{L(b) - L(s) + \frac{1}{2}(\theta - b)^{\top} H_b(\theta - b)}{T_b}\right] d\theta \tag{53}$$

$$=\hat{D}_b^{-1} \exp\left(\frac{L(b) - L(s)}{T_b}\right) \sqrt{\frac{2\pi T_b}{|H_b|}}.$$
(54)

Besides the temperature correction  $T = \frac{D}{\gamma M}$ , this result of J in Momentum also differs from SGD by the effective diffusion correction  $\frac{\hat{D}_b}{D_b}$ . The effective diffusion correction coefficient is given by

$$\frac{\hat{D}_i(\theta)}{D_i(\theta)} = \frac{1 - \sqrt{1 - \frac{4H_i(\theta)}{\gamma^2 M}}}{\frac{2H_i(\theta)}{\gamma^2 M}}.$$
(55)

Based on the formula of the one-dimensional probability current and flux, we obtain the high-dimensional flux escaping through b:

$$\int_{S_{k}} J \cdot dS \tag{56}$$

$$= J_{1d} \int_{S_b} \exp\left[-\frac{\gamma M}{2} (\theta - b)^{\top} [D_b^{-\frac{1}{2}} H_b D_b^{-\frac{1}{2}}]^{\perp e} (\theta - b)\right] dS$$
 (57)

$$=J_{1d}\frac{(2\pi\gamma M)^{\frac{n-1}{2}}}{(\prod_{i\neq e}(D_{bi}^{-1}H_{bi}))^{\frac{1}{2}}}$$
(58)

$$= \frac{\exp\left(\frac{L(a) - L(s)}{T_{ae}}\right) P(a) \frac{(2\pi\gamma M)^{\frac{n-1}{2}}}{(\prod_{i \neq e} (D_{bi}^{-1} H_{bi}))^{\frac{1}{2}}}}{\hat{D}_{be}^{-1} \exp\left(\frac{L(b) - L(s)}{T_{be}}\right) \sqrt{\frac{2\pi T_{be}}{|H_{be}|}}}$$
(59)

where  $[\cdot]^{\perp e}$  indicates the directions perpendicular to the escape direction e. Based on the results of Step 1 and Step 2, we have

$$\tau = \frac{P(\theta \in V_a)}{\int_{S_b} J \cdot dS} \tag{60}$$

$$=P(a)\frac{(2\pi\gamma M)^{\frac{n}{2}}}{\det(D_a^{-1}H_a)^{\frac{1}{2}}}\frac{\hat{D}_{be}^{-1}\exp\left(\frac{L(b)-L(s)}{T_{be}}\right)\sqrt{\frac{2\pi T_{be}}{|H_{be}|}}}{\exp\left(\frac{L(a)-L(s)}{T_{ae}}\right)P(a)\frac{(2\pi\gamma M)^{\frac{n-1}{2}}}{(\prod_{i,j}(D_{i-1}^{-1}H_{bi}))^{\frac{1}{2}}}}$$
(61)

$$= \frac{1}{\hat{D}_{be}} 2\pi \frac{D_{be}}{|H_{be}|} \exp\left[\frac{2\gamma MB\Delta L}{\eta} \left(\frac{s}{H_{ae}} + \frac{(1-s)}{|H_{be}|}\right)\right]$$
(62)

$$=\pi \left[ \sqrt{1 + \frac{4|H_{be}|}{\gamma^2 M}} + 1 \right] \frac{1}{|H_{be}|} \exp \left[ \frac{2\gamma M B \Delta L}{\eta} \left( \frac{s}{H_{ae}} + \frac{(1-s)}{|H_{be}|} \right) \right]. \tag{63}$$

We have replaced the eigenvalue of  $H_b$  along the escape direction by its absolute value.  $\Box$ 

#### A.4 Proof of Proposition 2

*Proof.* The proof closely relates to the proof of 3.2. We only need replace the standard learning rate by the adaptive learning rate  $\hat{\eta} = \eta V^{-\frac{1}{2}}$ , and set  $\gamma M = 1$ . Particularly,

$$D_{adam} = DV^{-\frac{1}{2}} = \frac{\eta[H]^{+}V^{-\frac{1}{2}}}{2B} = \frac{1}{2}\eta\sqrt{\frac{[H]^{+}}{B}}.$$
 (64)

We introduce  $\hat{\eta} = \eta V^{-\frac{1}{2}}$  into the proof of 3.2, and obtain

$$\tau = \frac{P(\theta \in V_{a})}{\int_{S_{b}} J \cdot dS}$$

$$= \left[ \frac{|\det(D_{b}^{-1}V_{b}^{\frac{1}{2}}H_{b})|}{\det(D_{a}^{-1}V_{a}^{\frac{1}{2}}H_{a})} \right]^{\frac{1}{2}} \pi \left[ \sqrt{1 + \frac{4|H_{be}|}{\gamma^{2}M}} + 1 \right] \frac{1}{|H_{be}|} \exp \left[ \frac{2\gamma MB\Delta L}{\eta} \left( \frac{s}{V_{ae}^{-\frac{1}{2}}H_{ae}} + \frac{(1-s)}{V_{be}^{-\frac{1}{2}}|H_{be}|} \right) \right]$$

$$= \pi \left[ \sqrt{1 + \frac{4\eta\sqrt{B|H_{be}|}}{1-\beta_{1}}} + 1 \right] \frac{|\det(H_{a}^{-1}H_{b})|^{\frac{1}{4}}}{|H_{be}|} \exp \left[ \frac{2\sqrt{B}\Delta L}{\eta} \left( \frac{s}{\sqrt{H_{ae}}} + \frac{(1-s)}{\sqrt{|H_{be}|}} \right) \right] .$$
(67)

#### A.5 Proof of Proposition 4

*Proof.* The proof closely relates to the proof of 3.2. We only need introduce the mass matrix M and the dampening matrix  $\gamma$ . Fortunately,  $\gamma M = I$ . Thus we directly have the result from the proof of 3.2 as:

$$\tau = \frac{P(\theta \in V_a)}{\int_{S_b} J \cdot dS} \tag{68}$$

$$=\pi \left[ \sqrt{1 + \frac{4|H_{be}|}{\gamma^2 M}} + 1 \right] \frac{1}{|H_{be}|} \exp \left[ \frac{2\gamma M B \Delta L}{\eta} \left( \frac{s}{H_{ae}} + \frac{(1-s)}{|H_{be}|} \right) \right]. \tag{69}$$

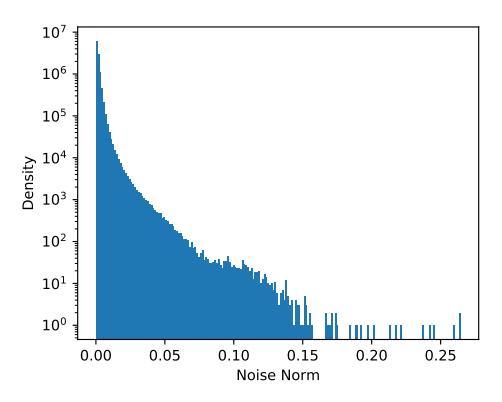
As  $M = \eta(I - \mu)^{-1}$ ,  $\gamma = \eta^{-1}(I - \mu)$ , and  $I - \mu = \frac{n\beta_0}{\|V\|_1}V$ , we obtain the result:

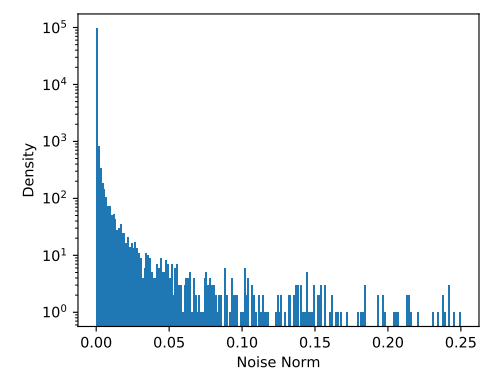
$$\tau = \pi \left[ \sqrt{1 + \frac{4\eta \sum_{i=1}^{n} |H_{bi}|}{\beta_0 n}} + 1 \right] \frac{1}{|H_{be}|} \exp \left[ \frac{2B\Delta L}{\eta} \left( \frac{s}{H_{ae}} + \frac{(1-s)}{|H_{be}|} \right) \right]$$
(70)

# **B** Discussion on Approximation Assumptions

In the diffusion theoretical framework, Xie et al. (2020) has well discussed why Assumption 3 and Assumption 4 are still reasonable in deep learning domain. We review the main viewpoints. Assumption 3 and Assumption 4 are widely used in Kramers Escape Problem across multiple fields, such as statistical physics, chemistry, and biology (Van Kampen, 1992). Quasi-Equilibrium Assumption is weaker and more useful than the common stationary assumption. Under the stationary assumption, the probability current is zero at any point. There are no probability flux connecting different loss valleys. Little knowledge about flat minima selection can be obtained under the stationary assumption. Under Quasi-Equilibrium Assumption, probability density P can behave like a stationary distribution only inside valleys, but density transportation across valleys is dynamic. Under Assumption 3,  $P(\theta,t)$  has locally reached the stationary distribution  $P(\theta)$  around critical points, while the distribution of different valleys may have not reached the stationary distribution. We can predict the probability of minima selection by modeling the probability flux and the probability volume of a loss valley.

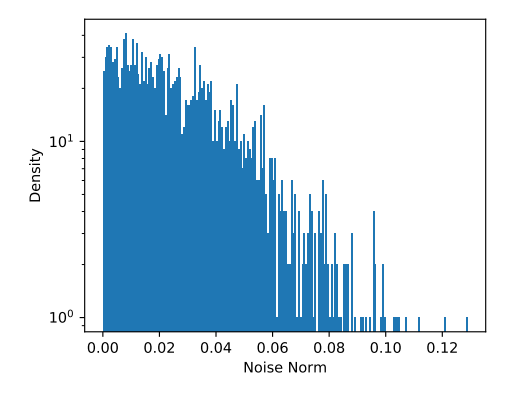
Low Temperature Assumption is always justified when  $\frac{\eta}{B}$  is small. Numerically, 6-sigma rule  $(\Delta L > \frac{3D_e}{\gamma M})$  already provides good approximation in Gaussian distribution. Under Assumption 1 and Assumption 4, we can apply the second order Taylor approximation,

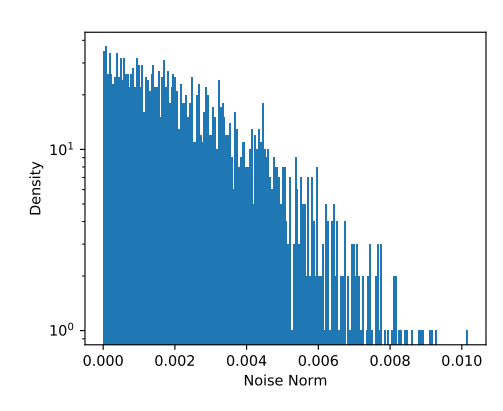




(a) Gradient Noise of one minibatch across parameters







(c) Gradient Noise of one parameter across minibatches

(d) Gaussian noise

Figure 4: The Stochastic Gradient Noise Analysis. The histogram of the norm of the gradient noises computed with ResNet18 on CIFAR-10. In Subfigure (a), we follow Simsekli et al. (2019) and compute "stochastic gradient noise" across parameters. In Subfigure (c), we follow the usual definition and compute stochastic gradient noise across minibatches. Obviously, the real stochastic gradient noise is more like Gaussian noise rather than Lévy noise.

and the probability densities concentrates around minima and critical escape paths. The probability density inside a loss valley is like the water in a lake, while the probability flux along the escape path is the water flux in a river. Thus we mathematical predict flat lake has more water.

# C The Gradient Noise Analysis

In Figure 4, we reveal the difference between gradient noise of one minibatch across parameters and gradient noise of one parameters across minibatches. Obviously, gradient noise of one minibatch across parameters which Simsekli et al. (2019) studied is Lévy noise. This is based on the isotropic assumption that gradients of all parameters at one iteration must obey the same one distribution. In contrast, gradient noise of one parameters across minibatches which is the usual noise in Langevin Dynamics is Gaussian noise.

We also emphasize that a few researchers are confusing stochastic gradient and stochastic gradient noise. Stochastic gradient is the gradient of stochastic minibatches, while stochastic

gradient noise is the gradient of stochastic minibatches minus the gradient of the whole training dataset.

In Figure 1, we validate the relation between gradient noise covariance and Hessian presented in Equation 5. We particularly choose a randomly initialized mode so that the model is not near critical points. We notice that Equation 5 still approximately hold especially along the directions of small eigenvalues of Hessian. Fortunately, the small eigenvalue of Hessians is exactly the case we are interested in, as small Hessian eigenvalues is the main problem in saddle-point escaping fast.

#### D Experimental Details

#### D.1 Experimental Settings

Hyperparameter Setting: We select the optimal learning rate for each experiment from  $\{0.00001, 0.0001, 0.001, 0.01, 0.1, 1, 10\}$ . For the learning rate schedule, the learning rate is divided by 10 at the epoch of  $\{80, 160\}$  for CIFAR-10,  $\{100, 150\}$  for CIFAR-100, and  $\{30, 60, 90\}$  for ImageNet. The batch size is set to 128 for CIFAR-10/CIFAR-100, and is set to 256 for ImageNet. The weight decay is set to 0.0005 for CIFAR-10/CIFAR-100, and is set to 0.0001 for ImageNet, except that AdamW uses 0.1 for CIFAR-10/CIFAR-100 and ImageNet. As for other optimizer hyperparameters, we directly apply the default setting of each optimizer:  $\beta_0 = 0.1, \beta_2 = 0.99, \epsilon = 1e - 3$  for Adai,  $\beta_1 = 0.9, \beta_2 = 0.999, \epsilon = 1e - 8$  for Adam, and  $\beta = 0.9$  for SGD with Momentum.

**Data Preprocessing:** For CIFAR-10/CIFAR-100, we perform the usual per-pixel mean subtraction, horizontal random flip, and  $32 \times 32$  random crops after padding with 4 pixels on each side. For ImageNet, we perform the usual per-pixel mean subtraction, horizontal random flip, and the resized random crops where the random size (of 0.08 to 1.0) of the original size and a random aspect ratio (of 3/4 to 4/3) of the original aspect ratio is made.

#### D.2 More Experimental Results

In Figure 5, we present the optimal curves of ResNet18 and VGG16 on CIFAR-10.

In Figure 6, we present the optimal curves of DenseNet121 and GoogLeNet on CIFAR-100.

In Figure 7, we present the optimal curves of ResNet50 on ImageNet.

In Figure 8, we show that Adai has better convergence performance than Adam. When they converges similarly fast, Adai converges in a lower training loss in the end. When they converge in a similarly low training loss, Adai converges fast in the beginning.

## E The Mean Escape Time Analysis

**Data Set:** We generate 50000 Gaussian samples as the training data set, where  $x \sim \mathcal{N}(0, 4I)$ . **Hyperparameters**: The batch size is set 10. No weight decay. The learning rate: 0.001 for Adai, 0.0001 for Momentum (with  $\beta = 0.9$ ), and 0.03 for Adam.

**Test Function:** Styblinski-Tang Function is a commonly used function in nonconvex optimization, written as

$$f(\theta) = \frac{1}{2} \sum_{i=1}^{N} (\theta_i^4 - 16\theta_i^2 + 5\theta_i).$$

We use 10-dimensional Styblinski-Tang Function as the test function, and Gaussian samples as training data.

$$L(\theta) = f(\theta - x),$$

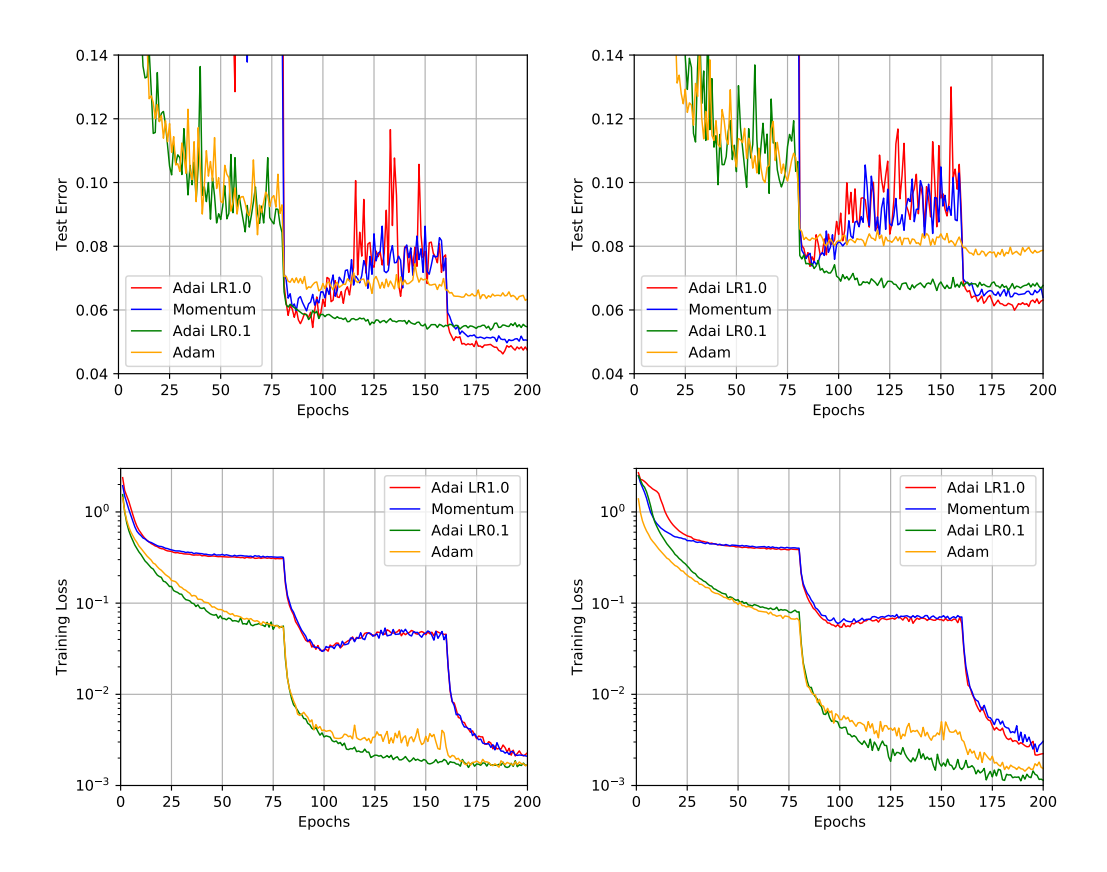


Figure 5: Left: ResNet18 on CIFAR-10. Right: VGG16 on CIFAR10. Top: Test Error. Bottom: Training Loss. Hyperparameters for Left:  $\eta=0.0001$  for Adam,  $\eta=0.1$  for SGD with Momentum. Hyperparameters for Right:  $\eta=0.0001$  for Adam,  $\eta=0.1$  for SGD with Momentum.

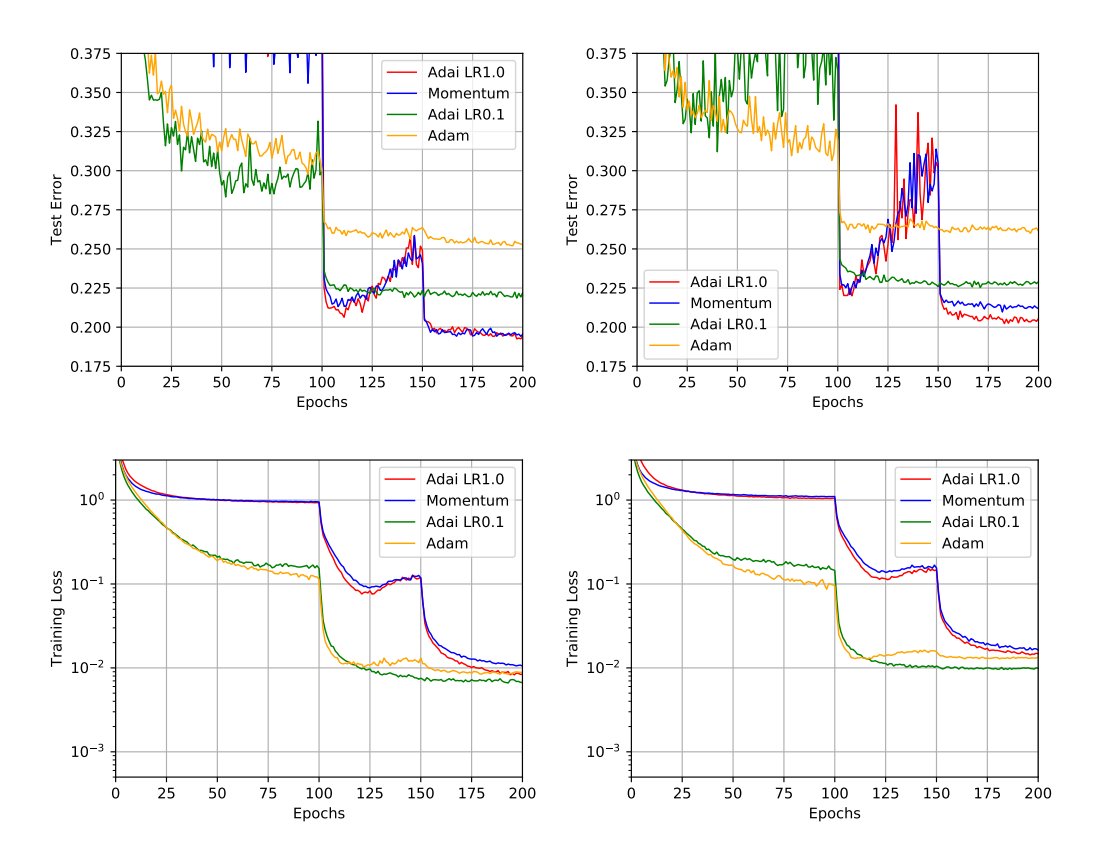


Figure 6: Left: DenseNet121 on CIFAR-100. Right: GoogLeNet on CIFAR100. Top: Test Error. Bottom: Training Loss. Hyperparameters for Left:  $\eta=0.0001$  for Adam,  $\eta=0.1$  for SGD with Momentum. Hyperparameters for Right:  $\eta=0.0001$  for Adam,  $\eta=0.1$  for SGD with Momentum.

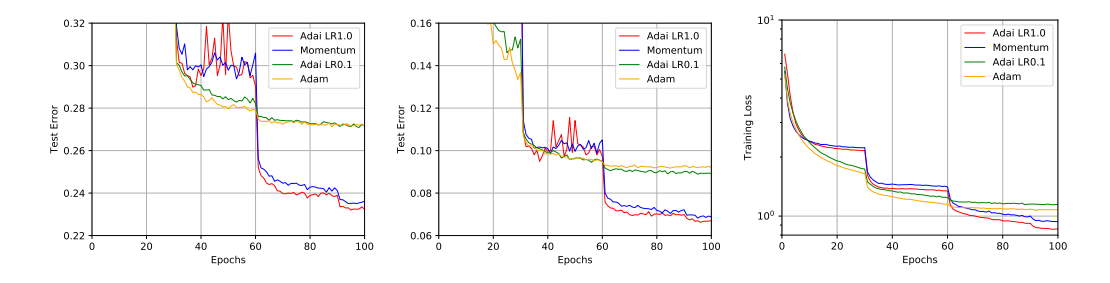


Figure 7: ResNet50 on ImageNet. Left: Top 1 Test Error. Middle: Top 5 Test Error. Right: Training Loss. Hyperparameters:  $\eta = 0.0001$  for Adam,  $\eta = 0.1$  for SGD with Momentum.

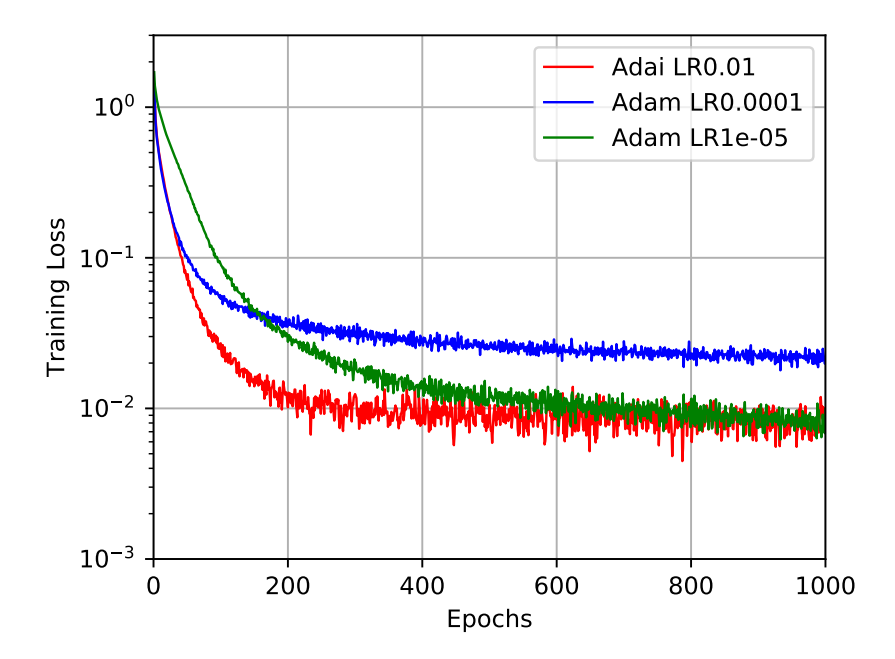


Figure 8: VGG16 on CIFAR-10. We fix the learning rate, and train the models for 1000 epochs. When they converge similarly fast, Adai converges in a lower training loss in the end. When they converge in a similarly low training loss, Adai converges fast in the beginning.

where data samples  $x \sim \mathcal{N}(0,4I)$ . The one-dimensional Styblinski-Tang Function has one global minimum located at a=-2.903534, one local minimum located at d, and one saddle point b=0.156731 as the boundary separating Valley  $a_1$  and Valley  $a_2$ . For a n-dimensional Styblinski-Tang Function, we initialize parameters  $k\theta_{t=0}=(-2.903534,\cdots,-2.903534)$ , and set the valley's boundary as  $\theta_i<0.156731$ , where i is the dimension index. We record the number of iterations required to escape from the valley to the outside of valley. The setting 1 does not need labels.

**Observation**: we observe the number of iterations from the initialized position to the terminated position. As we are more interested in the number of iterations than "dynamical time" in practice, we use the number of iterations to denote the mean escape time and ignore the time unit  $\eta$  in "dynamical time". We repeat experiments 100 times to estimate the escape rate  $\Gamma$  and the mean escape time  $\tau$ . As the escape time is approximately a random variable obeying an exponential distribution,  $t \sim Exponential(\Gamma)$ , the estimated escape rate can be written as

$$\Gamma = \frac{100 - 2}{\sum_{i=1}^{100} t_i}.\tag{71}$$

The 95% confidence interval of this estimator is

$$\Gamma(1 - \frac{1.96}{\sqrt{100}}) \le \Gamma \le \Gamma(1 + \frac{1.96}{\sqrt{100}}).$$
 (72)